DOI: 10.1002/asia.200600017

Periodic Trends in the Agostic Interaction in Zirconium and Hafnium Methylidene Hydride Halide Complexes

Han-Gook Cho,[b] Tae-Hyun Kim,[b] and Lester Andrews*[a]

Abstract: The reactions of methyl chloride and bromide with laser-ablated Zr and Hf atoms during deposition in excess Ne, Ar, or Kr are investigated, and the products are examined by matrix IR spectroscopy and density functional theory calculations. The methylidene complexes, [CH_2=MHX] (M = Zr and Hf, X = Cl and Br), are formed along with the methyl metal halide complexes, [CH_3–MX]. The amounts of both types of complexes increase upon photolysis and in the early stages of annealing. Two sets of methylidene absorptions observed in Ar and Kr matrices form a persistent photoreversible system. The most stable C_1 and slightly higher energy planar structures of the methylidene complex in the singlet ground state trapped in the matrix reproduce the characteristics of the two sets of absorptions. Agostic distortion of the methylidene complexes decreases in the order Ti, Zr, Hf and increases in the order F, Cl, and Br; the C=Zr and Zr–H stretching frequencies increase, and the bonds become shorter. This observation favors the characterization of the agostic interaction as a reorganization of charge.

Keywords: agostic interactions · alkylidenes · density functional calculations · hafnium · zirconium

Introduction

Alkylidene complexes of Group IV, V, and VI transition metals are important reagents in the synthesis of organometallic compounds, and many of these complexes are agostic.[1] Laser-ablated Ti, Zr, and Hf atoms readily form methylidene and methyl metal halide complexes ([CH_2=MHX] and [CH_3–MX], X = H or F), and agostic distortion is observed in these simplest-possible methylidene complexes in IR spectra as well as in calculated structures.[2–7] Moreover, photoreversible conversions are observed in the zirconium systems,[6,7] which most likely involve the singlet and triplet CH_2=ZrH_2 or CH_2=ZrHF states, and give two different matrix-cage configurations. On the other hand, photoreversible conversion occurs in the Ti systems, through migration of an α hydrogen atom in the [CH_3–TiX] and [CH_2=TiHX] complexes.[2,3,8] Furthermore, methyl chloride and bromide react even more readily than methane and methyl fluoride with laser-ablated transition metals.[8] The observed C=Ti stretching frequency of the methylidene complexes increases in the order F, Cl, and Br, and calculations also show that the carbon–metal bond length decreases and the molecular structure becomes more agostic with increasing halogen size.

The transition metals in Group VI form not only the methyl halide and methylidene complexes but the methylidyne ([CH≡MH_2X]) complexes as well, and the products are also photoreversible by migration of an α hydrogen atom.[9–12] The transition metals in Group V also produce the methylidene and methyl halide complexes and form anionic methylidyne complexes ([CH≡MH_2X]$^-$).[13,14] These simple high-oxidation-state complexes are model compounds for the much larger Schrock carbene and carbyne complexes,[1] which are important for C–H activation of hydrocarbons, for catalysis of metathesis reactions of unsaturated compounds, and for understanding the agostic interaction.[1,15–21]

If the trend of increasing agostic bonding effects with increasing halogen size found for the [CH_2=TiHX] complexes[8] can be generalized for other metals, more fundamental understanding of the agostic interaction may be obtained. The agostic interaction was featured in two excellent recent review articles.[20,21] The original term was used to describe coordinative interactions between C–H bonds and transition-metal centers in organometallic compounds.[18] Steric effects on this interaction have also been consid-

[a] Prof. Dr. L. Andrews
Department of Chemistry, University of Virginia
P. O. Box 400319, Charlottesville, VA 22904-4319 (USA)
Fax: (+1) 434-924-3710
E-mail: lsa@virginia.edu

[b] Prof. Dr. H.-G. Cho, Prof. Dr. T.-H. Kim
Department of Chemistry
University of Incheon, 402-749 (South Korea)

WILEY InterScience DISCOVER SOMETHING GREAT
© 2006 Wiley-VCH Verlag GmbH & Co. KGaA, Weinheim

ered.[20] Scherer and McGrady recently characterized the agostic interaction as negative hyperconjugative delocalization of M–C bonding electrons in order to stabilize the organometallic system.[21] Accordingly, the comparison of F, Cl, and Br substituents in [CH_2=MHX] complexes will test these models of the agostic interaction.

In this investigation, reactions of laser-ablated Zr and Hf atoms with methyl chloride and bromide diluted in Ne, Ar, or Kr were carried out, and the products isolated in solid matrices were investigated by means of IR spectroscopy. Results indicate that two major reaction products, the methylidene and methyl metal halide complexes, are formed on the basis of the vibrational characteristics and their variations upon photolysis and annealing. These results are compared with earlier products of methyl fluoride reactions[4,6] to examine periodic trends in the agostic interaction in these simple methylidene complexes.

Results and Discussion

Experimental and theoretical characterization of the products of Zr and Hf atom reactions with CH_3Cl and CH_3Br will be presented in turn, followed by a consideration of the trends in agostic bonding.

Zr + CH_3Cl

Figure 1 shows the IR spectra in the regions of 1650–1500 and 800–430 cm^{-1} for laser-ablated Zr atoms codeposited with Ar/CH_3Cl at 8 K and their variations upon photolysis and annealing. In the region of 1650–1500 cm^{-1}, strong product absorptions are found at 1554.0 and 1570.5 cm^{-1} (marked **I** and **II**). Deuteration of the precursor resulted in large frequency shifts of −438.5 and −442.8 cm^{-1} (H/D isotopic ratios for both 1.393), respectively, as shown in Figure 2, thus indicating that these are Zr–H stretching absorptions. In earlier studies, the hydrogen stretching absorptions of zirconium hydrides (ZrH_x), which are not observed in this study, are also located in the same frequency region.[24]

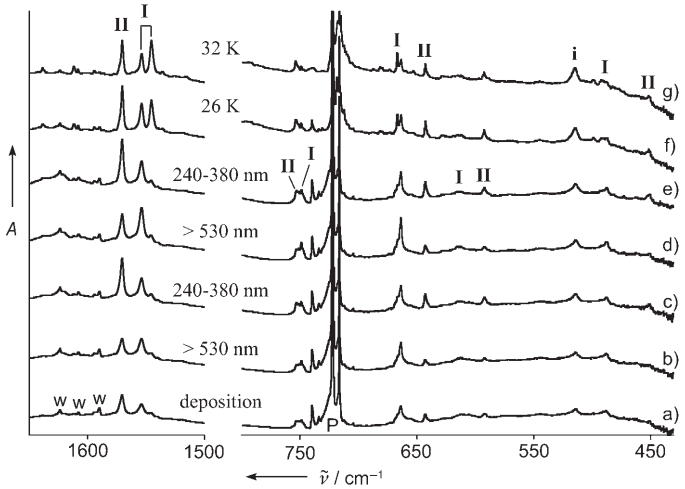

Figure 1. IR spectra in the regions of 1500–1650 and 430–800 cm^{-1} for laser-ablated Zr atoms codeposited with Ar/CH_3Cl at 8 K. a) Zr + CH_3Cl (0.2%) in Ar codeposited for 1 h. b) After broadband photolysis with a filter ($\lambda > 530$ nm) for 20 min. c) After broadband photolysis with a near-UV transmitting filter ($240 < \lambda < 380$ nm) for 20 min. d) After second photolysis with a filter ($\lambda > 530$ nm) for 20 min. e) After second photolysis with a near-UV transmitting filter ($240\ nm < \lambda < 380$ nm) for 20 min. f) After annealing to 26 K. g) After annealing to 32 K. **I** and **II** refer to the absorption group arising from [CH_2=ZrHCl], and **i** refers to the absorption from [CH_3–ZrCl]. P = precursor, W = water.

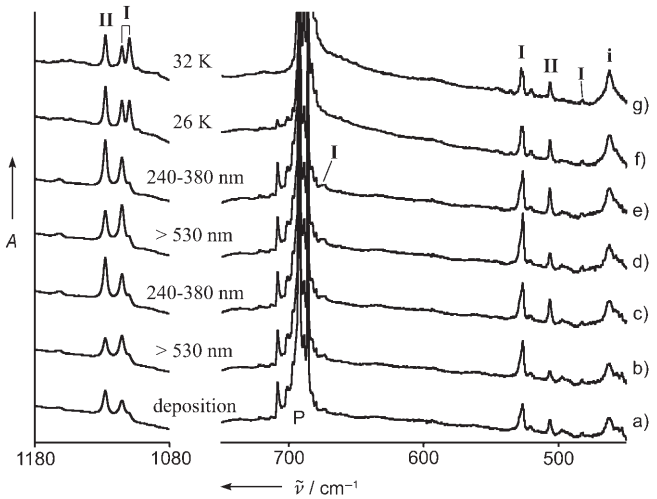

Figure 2. IR spectra in the regions of 1080–1180 and 450–750 cm^{-1} for laser-ablated Zr atoms codeposited with Ar/CD_3Cl at 8 K. a) Zr + CD_3Cl (0.5%) in Ar codeposited for 1 h. b) After broadband photolysis with a filter ($\lambda > 530$ nm) for 30 min. c) After broadband photolysis with a near-UV transmitting filter ($240 < \lambda < 380$ nm) for 30 min. d) After second photolysis with a filter ($\lambda > 530$ nm) for 30 min. e) After second photolysis with a near-UV transmitting filter ($240\ nm < \lambda < 380$ nm) for 30 min. f) After annealing to 26 K. g) After annealing to 32 K. **I** and **II** refer to the absorption group arising from [CH_2=ZrDCl], and **i** refers to the absorption from [CD_3–ZrCl].

The strong metal–hydrogen stretching absorptions even at low concentrations of CH_3Cl (0.2%) indicate that C–H activation readily occurs in the reaction of Zr with CH_3Cl. It was previously reported that CH_3F is more reactive than CH_4 towards Zr probably because the lone electron pairs of the halogen atom attract the electron-deficient metal atom. Apparently CH_3Cl is even more reactive than CH_3F towards the transition metal.

Photolysis with a broadband Hg lamp and a filter ($\lambda >$ 530 nm) led to increase in **I** and decrease in **II**. On the other hand, irradiation with a near-UV transmitting filter ($240 < \lambda < 380$ nm) led to a large increase in **II**, whereas **I** only slightly grew. Irradiation with visible light of short wavelength ($380 < \lambda < 530$ nm) did not produce any observable change in the spectra. After the first near UV irradiation, increase of one hydrogen stretching absorption was always accompanied with decrease of the other, while the total absorption intensity of the two absorptions continuously increased. **I** increased upon irradiation with visible light

 © 2006 Wiley-VCH Verlag GmbH & Co. KGaA, Weinheim

(>530 nm), whereas **II** decreased. UV irradiation reversed the effect. Almost-identical photoreversible variations in the intensities of the **I** and **II** absorptions were also observed in a Kr matrix as shown in Figure 3, in which the frequencies

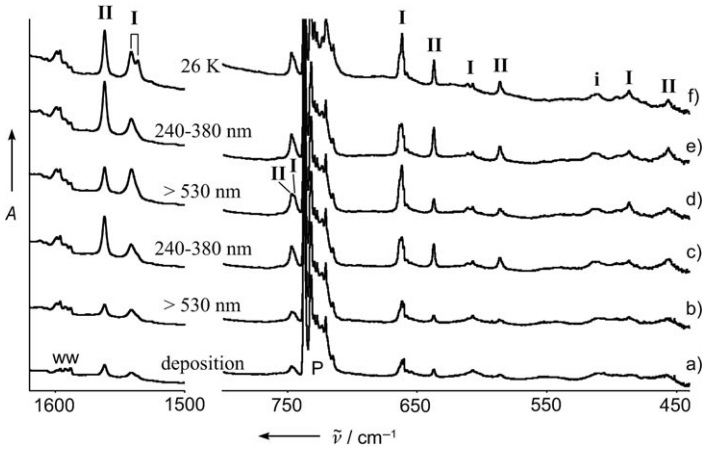

Figure 3. IR spectra in the regions of 1500–1650 and 430–800 cm^{-1} for laser-ablated Zr atoms codeposited with Kr/CH_3Cl at 12 K. a) Zr + CH_3Cl (0.5%) in Kr codeposited for 45 min. b) After broadband photolysis with a filter ($\lambda > 530$ nm) for 20 min. c) After broad-band photolysis with a near-UV transmitting filter ($240 < \lambda < 380$ nm) for 20 min. d) After second photolysis with a filter ($\lambda > 530$ nm) for 20 min. e) After second photolysis with a near-UV transmitting filter (240 nm $< \lambda <$ 380 nm) for 20 min. f) After annealing to 26 K. **I** and **II** refer to the absorption group arising from [CH_2=ZrHCl], and **i** refers to the absorption from [CH_3–ZrCl].

of both absorptions were slightly lower and their difference in frequency slightly larger (20.5 cm^{-1}). On the other hand, only one metal–hydrogen stretching absorption was observed in the Ne matrix spectrum, at 1574.2 cm^{-1} (not shown).

In the early stages of annealing, up to 26 K, the total intensity of the metal–hydrogen stretching absorption increased; in particular, the absorption at 1545.6 cm^{-1}, also marked **I** and is very weak in the original spectrum after deposition, increased dramatically (Figure 1). This absorption grew further upon annealing up to 32 K, whereas the absorptions at 1554.0 and 1570.5 cm^{-1} decreased. In the spectra shown in Figures 1–3, the **I** absorptions exhibit more site splittings than those of **II**. This cluster of bands is due to a simple Zr–H stretching mode in a molecule with one Zr–H bond that can exist in two very similar structures or matrix-trapping configurations.

The present results indicate that a new molecule with one Zr–H bond is formed in the reaction of Zr with CH_3Cl, and therefore, the singlet methylidene complex [CH_2=ZrHCl], which is the most stable among the plausible products,[6] must be considered. This is consistent with the previous studies of Zr reactions with CH_4 and CH_3F.[6,7] Photolysis also initiates the reaction of Zr atoms with CH_3Cl located nearby in the matrix, and increases the total concentration of the two absorptions. Moreover, the persistent photoreversibility of the two hydrogen stretching absorptions 16.5 cm^{-1} apart suggests that the two metal–hydrogen stretching absorptions actually arise from the methylidene complex in two substantially different conditions. Upon photolysis, an increase in concentration of the methylidene complex in one condition leads to a decrease in concentration in the other, which involves the excited electronic states of the methylidene complex.[5] For example, the lowest triplet state has a planar structure, which in turn leads to rearrangement of the matrix configuration around the complex.

Similar changes in absorption intensities upon photolysis with visible and near-UV light were also observed in the region of 800–430 cm^{-1} (Figure 1). The absorptions marked **I** at 749.1, 666.9, 663.6, 614.9, 612.1, and 487.2 cm^{-1} increased and decreased upon irradiation with visible ($\lambda >$ 530 nm) and near-UV ($240 < \lambda < 380$ nm) light, respectively. On the other hand, the absorptions marked **II** at 753.4, 642.7, 592.2, and 450.6 cm^{-1} decreased and increased upon irradiation with visible and near-UV light, respectively. Almost-identical variations in intensity were observed in the Kr matrix spectra shown in Figure 3.

The counterparts of the **I** and **II** absorptions at 749.1 and 753.4 cm^{-1} in the spectra of Zr + CD_3Cl were much weaker, with frequency shifts of about −70 cm^{-1} (H/D isotopic ratio ≈1.11) (Figure 2). On the basis of the frequencies, isotopic shifts, and previous results, they are attributed mostly to the C=Zr stretching mode. The stronger absorptions at 663.6 and 642.7 cm^{-1} (20.9 cm^{-1} apart) showed deuterium shifts of −137.1 and −136.5 cm^{-1} (H/D isotopic ratio of 1.260 and 1.270), respectively. They are assigned to the CH_2 wagging mode of the methylidene complex. The absorptions at 614.9 (**I**) and 592.2 cm^{-1} (**II**) also clearly showed reversible variations in intensity upon irradiation with visible and UV light. The deuterium counterpart of the **I** absorption was observed at 482.6 cm^{-1} (the deuterium shift and H/D ratio are −132.3 cm^{-1} and 1.274, respectively). On the basis of the frequency, large deuterium shift, and calculation results, we assign the absorptions to the C–Zr–H bending mode of the methylidene complex.

At even lower frequency, two more absorptions that showed reversible variations in intensity were observed in the CH_3Cl spectra at 487.2 (**I**) and 450.6 cm^{-1} (**II**) (36.6 cm^{-1} apart), whereas the deuterium counterparts were not observed due to their low frequencies. On the basis of the frequencies and previous results, they are attributed to the CH_2 twisting mode. The observed **I** and **II** absorptions reveal that the methylidene complex (CH_2=ZrHCl) is a major reaction product of Zr with CH_3Cl, which is consistent with reactions of laser-ablated Zr with methyl fluoride reported previously.[6]

The observed frequencies in the Ne, Ar, and Kr matrix spectra of Zr + CH_3Cl are listed in Table 1, and new results for the Zr + CH_3F reaction are given in Table 2. The Ar matrix frequencies of the methylidene and methyl metal halide complexes are compared with calculated values in Tables 3 and 4, respectively. The two sets of absorptions (**I**

 © 2006 Wiley-VCH Verlag GmbH & Co. KGaA, Weinheim

Table 1. Observed product absorptions from reactions of Zr with methyl halides.[a]

Zr+CH_3Cl					Zr+CD_3Cl			Zr+CH_3Br		Zr+CD_3Br		Description
Ne	Ar		Kr		Ne	Ar		Ar		Ar		
	I	**II**	**I**	**II**		**I**	**II**	**I**	**II**	**I**	**II**	
1574.2	**1554.0**, 1545.6	1570.5	**1541.6**, 1536.2	1562.1	1129.8	**1115.5**, 1110.0	1127.7	**1556.6**, 1546.5	1573.7	**1117.1**, 1110.5	1129.9	Zr–H stretch
754.0	749.1	753.4	744.8	747.0	682.9	676.9		**752.9**, 741.2	756.3	675.8	686.4	C=Zr stretch
670.1	666.9, **663.6**	642.7	663.5, **661.9**	637.1	531.3	527.8, **526.5**	506.2	665.0, **661.9**	643.0	527.8, **525.2**	506.9	CH_2 wag
619.6	**614.9**, 612.1	592.2	611.1, **607.2**	586.1	475.7	482.6		622.6, **614.8**		484.0		C–Zr–H bend
483.5	487.2	450.6	486.7	456.2				494.4, **482.7**	453.6			CH_2 twist
1384.8	1374.3		1370.8		996.0	993.8		1370.1				CH_2 bend
1137.6	1131.7		1133.5, **1129.3**		895.3	892.3		1129.0		889.6		CH_3 deform
515.7	513.9		514.3		465.4	462.3		514.2		461.4		C–Zr stretch

[a] All frequencies are in cm^{-1}. Stronger absorptions are in bold. The methylidene product is listed in the top portion followed by the insertion product.

Table 2. Observed product absorptions from reaction of Zr with CH_3F isotopomers.[a]

Zr+CH_3F					Zr+CD_3F		Zr+$^{13}CH_3F$		Description
Ne	Ar		Kr		Ar		Ar		
	I	**II**	**I**	**II**	**I**	**II**	**I**	**II**	
1579.2	1537.8, 1532.4	1551.3	1522.3	1541.6	1104.3	1114.4	1537.8, 1532.4	1551.3	Zr–H stretch
743.8	740.0	742.0	732.8	734.8	641.8	645.2	721.5	723.2	C=Zr stretch
688.5	669.4	642.2	666.9	636.0	534.0	503.7	663.7	638.4	CH_2 wag
643.9	633.5	631.0	628.1	625.6	607.5	605.6	632.4	629.1	Zr–F stretch
519.0	501.7	513.2	499.9	509.4				501.0	C–Zr–H bend
	1115.8		1114.5		890.5		1106.4		CH_3 deform
609.2	611.0		605.0		610.8		610.9		Zr–F stretch
518.8	489.2								C–Zr stretch

[a] All frequencies are in cm^{-1}. The methylidene product is listed in the top portion followed by the insertion product.

and **II**) were clearly observed in the Ar- and Kr-matrix spectra as shown in Figures 1–3, whereas only one set of absorptions was observed in the Ne matrix spectra. The frequency difference between **I** and **II** was in general larger in the Kr-matrix spectra.

The frequency of the Zr–H stretching **I** absorption was lower than that of the **II**. The frequency difference of the C=Zr stretching absorption pair was far smaller than those of the H stretching and bending modes, thus resulting in heavy overlap. Furthermore, the H bending (CH_2 wagging, C–Zr–H bending, and CH_2 twisting) absorption pairs showed larger frequency differences than the metal–hydrogen stretching pair. The largest frequency difference was observed from the CH_2 twisting absorptions ($\approx 37\ cm^{-1}$). Other than the Zr–H and C=Zr stretching frequencies, the **I** frequencies were all

Table 3. Observed and calculated fundamental frequencies for [CH_2=ZrHCl] and [CH_2=ZrHBr] in the ground electronic states (^1A).[a]

Description	CH_2=ZrHCl					CD_2=ZrDCl					CH_2=ZrHBr					CD_2=ZrDBr				
	Obs		Calcd		*I*	Obs		Calcd		*I*	Obs		Calcd		*I*	Obs		Calcd		*I*
	I	II	Planar	C_1		I	II	Planar	C_1		I	II	Planar	C_1		I	II	Planar	C_1	
C–H_b stretch			3184.6	3183.8	1			2355.1	2354.8	3			3185.1	3183.4	1			2355.6	2354.8	4
C–H_a stretch			2806.9	2821.1	7			2044.3	2054.1	3			2800.6	2806.4	6			2039.6	2043.4	3
Zr–H_c stretch	1554.0	1570.5	1622.2	1642.6	400	1115.5	1127.7	1154.3	1168.7	208	1556.6	1573.7	1623.5	1644.4	406	1117.1	1129.9	1155.1	1170.0	211
CH_2 scissors			1345.5	1338.4	21			1036.3	1033.4	22			1344.5	1340.1	22			1035.5	1033.9	24
C=Zr stretch	749.1	753.4	770.9	770.6	81	676.9		690.9	690.3	58	752.9	756.3	771.4	772.5	83	675.8	686.4	691.6	692.5	60
CH_2 wag	663.6	642.7	714.4	684.5	140	526.5	506.2	559.2	535.8	102	661.9	643.0	709.0	683.0	139	525.2	506.9	555.0	534.7	101
C–Zr–H_c bend	614.9	592.2	636.9	617.8	70	482.6		488.7	470.0	64	614.8		634.7	616.6	54	484.0		482.5	464.9	38
CH_2 twist	487.2	450.6	505.2	448.4	49			358.1	315.8	17	482.7	453.6	493.7	448.8	48			349.8	319.0	24
CH_2 rock			415.7	398.1	5			351.1	299.3	5			414.2	405.8	5			308.2	303.1	3
Zr–X stretch			357.2	365.7	66			308.4	360.2	50			256.2	264.2	49			251.0	258.7	35
Zr–H_c OOP bend			−78.6	215.9	87			63.2	163.3	37			−117.7	209.5	80			−87.0	156.4	38
C–Zr–X bend			135.9	110.0	33			122.6	96.9	30			120.8	98.8	23			108.6	87.3	21

[a] Observed frequencies were all measured in an Ar matrix. B3LYP/6-311++G(2d,p)/SDD(Zr) calculations were used. Frequencies and intensities are in cm^{-1} and $km\,mol^{-1}$, respectively, and ^{35}Cl and ^{79}Br were assumed in calculations. OOP = out of plane.

 © 2006 Wiley-VCH Verlag GmbH & Co. KGaA, Weinheim

Table 4. Observed and calculated fundamental frequencies of [CH_3ZrCl] and [CH_3ZrBr] isotopomers in the ground electronic states (^3A).[a]

Description	[CH_3ZrCl]				[CD_3ZrCl]			[CH_3ZrBr]				[CD_3ZrBr]		
	Obs	MP2	Calcd	*I*	Obs	Calcd	*I*	Obs	MP2	Calcd	*I*	Obs	Calcd	*I*
A′ CH_3 stretch		3164.1	3090.7	2		2281.1	1		3166.4	3088.0	2		2278.8	1
A′ CH_3 stretch		3002.3	2952.7	6		2119.8	1		3002.0	2948.6	6		2117.3	1
A′ CH_3 scissors		1408.3	1408.6	1		1022.4	1		1406.0	1408.1	1		1022.1	1
A′ CH_3 deform	1131.7	1146.3	1152.9	14	892.3	907.0	27	1129.0	1143.1	1154.7	14	889.6	908.7	28
A′ C–Zr stretch	513.9	526.8	512.1	40	462.3	449.9	40	514.2	527.9	512.5	44	461.4	450.6	41
A′ Zr–X stretch		380.5	389.2	76		371.4	70		308.5	368.8	37		298.2	37
A′ CH_3 rock		297.4	347.1	11		284.6	3		250.1	256.1	24		246.5	11
A′ C–Zr–X bend		82.0	94.9	1		86.7	1		71.1	81.3	1		73.5	1
A″ CH_3 stretch		3087.3	3011.3	4		2223.9	1		3087.4	3006.3	4		2220.0	1
A″ CH_2 bend	1374.3	1413.2	1418.7	7	993.8	1029.6	4	1370.1	1411.8	1418.4	7		1029.3	4
A″ CH_3 rock		329.2	353.8	5		264.0	3		321.3	354.4	5		264.1	3
A″ CH_3 distort		109.5	113.7	1		82.7	0		105.0	121.1	1		87.4	0

[a] Observed frequencies were all measured in an Ar matrix. B3LYP/6-311++G(2d,p)/SDD(Zr) calculations are given with MP2 added for comparison. Frequencies and intensities are in cm^{-1} and $km\,mol^{-1}$, respectively, and ^{35}Cl and ^{79}Br were assumed in calculations.

higher than those of **II**. These differences in frequency were unusually large, much larger than the frequency separations caused by typical matrix site effects.[26]

Earlier studies showed that the Ti–methylidene complexes in their ground singlet states have planar structures,[2,3,8] whereas the Zr– and Hf–methylidene complexes have C_1 structures with distorted CH_2 groups.[4–7] The predicted frequencies for this stable C_1 structure are listed in Table 3. (Frequencies computed with the large basis set are within 1–7 cm^{-1} and some are closer to the observed values.) Our BPW91, MP2, and CCSD calculations all showed that the only stable structure with all real frequencies of CH_2=ZrHCl in the ground singlet state is of C_1 geometry.

To examine the origins for the two absorption groups **I** and **II**, extensive calculations were carried out for the various conformations of the methylidene complex in the ground singlet state. The CH_2 distortion and H–C–Zr–Cl dihedral angles were varied systematically and the vibrational characteristics were calculated for the molecular structures. Interestingly, the planar structure, obtained by fixing the dihedral angles, has a low-frequency, imaginary out-of-plane Zr–H bending mode. In relation to the stable C_1 structure, this structure is only 0.4 $kJ\,mol^{-1}$ higher in energy, and the predicted Zr–H stretching frequency is about 20 cm^{-1} lower. On the other hand, the C=Zr stretching frequency is comparable to that of the C_1 structure, and the CH_2 wagging, C–Zr–H bending, and CH_2 twisting frequencies are higher, thus reproducing the characteristics of the **I** absorptions relative to those of the **II**. The frequencies predicted for the planar structure of CH_2=ZrHCl in the ground singlet state are listed along with the values for the C_1 structure in Table 3. No other conformation of the methylidene complex examined in this study reproduces as well as the planar structure the characteristics of both the **I** and **II** absorptions.

The lowest triplet state, which is 17 $kcal\,mol^{-1}$ higher in energy than the ground singlet state, has a planar structure with similar geometrical parameters other than the CH_2 distortion. On reaching the triplet state under photochemical excitation, the methylidene complex eventually relaxes down to the ground singlet state. We believe that the complex retains the planar structure because the matrix-cage configuration adjusts to the planar structure of the triplet state while the electronic energy is dissipated to the matrix, thus leading to the **I** absorptions. The Ar and Kr matrices are rigid enough to hold the so-formed planar structure even in the ground electronic state, but the Ne matrix is too soft to maintain the planar configuration. We suggest that the observed **I** and **II** absorptions arise from nearly planar (C_s) and pyramidal (C_1) structures of the singlet CH_2=ZrHCl complex trapped in the matrix. The absence of such a splitting for the CH_2=TiHX species is due to their planar ground-state structures.[2,3,8]

Other absorptions marked **i** were also observed at 513.9 and 462.3 cm^{-1} in Figures 1 and 2, respectively. They were relatively weak in the original spectrum after deposition, but increased upon photolysis, particularly with UV light. Upon annealing, the intensities of these absorptions increased about 3 times. They were much stronger in the spectra of Zr + CD_3Cl (Figure 2). Absorptions showing the same variation in intensity upon photolysis and annealing were observed at 1374.3 and 1131.7 cm^{-1} in the Zr + CH_3Cl spectra and at 993.8 and 892.3 cm^{-1} in the methyl region of the Zr + CD_3Cl spectra (not shown). The absorptions are assigned to the methyl halide complex, [CH_3–ZrCl], in the triplet ground state, and the frequencies are compared with the predicted values for the isotopomers in Table 4.

The absorptions of the triplet [CH_3–ZrF] complex observed in a previous study of Zr + CH_3F are much weaker.[6] The metal–halogen stretching absorption is expected to be the strongest among the product absorptions. The Zr–F stretching absorption shown in a previous study is in fact much weaker than the C–Zr stretching absorptions of [CH_3–ZrCl] shown in Figures 1 and 2 (the Zr–Cl stretching absorption was not observed due to its low frequency).[25] This indicates that more [CH_3–ZrCl] was produced relative to the fluorine counterpart.[6] Moreover, the absorptions from [CH_3–ZrF] disappeared completely upon UV photolysis, whereas more [CH_3–ZrCl] was produced in the process of photolysis and particularly annealing.

 © 2006 Wiley-VCH Verlag GmbH & Co. KGaA, Weinheim

CHEMISTRY
AN ASIAN JOURNAL

In the reaction of the transition metal with methyl halide, the insertion product, [CH_3–MX], is believed to be formed first, after which migration of the α hydrogen atom gives the methylidene complex.[2–14] Figures 1–3 show that the amount of methylidene complex also increases upon photolysis and annealing. Therefore, the much stronger [CD_3–ZrCl] relative to the [CH_3–ZrCl] absorptions indicate that α-D transfer is far less effective than α-H transfer, which is also the reason for the relatively weak absorptions of the deuterated methylidene complex.

$$Zr + CH_3Cl \xrightarrow{cold} [CH_3-ZrCl] \rightarrow [CH_2=ZrHCl] \quad (1)$$

$$Zr + CH_3Cl \xrightarrow{UV} [CH_3-ZrCl] \xrightarrow{UV} [CH_2=ZrHCl] \quad (2)$$

Figures 1–3 also show that the amount of [CH_2=ZrHCl] increases mostly upon near-UV photolysis, whereas that of [CH_3–ZrCl] increases mostly in the early stages of annealing. This indicates that UV excitation promotes both the insertion reaction to form [CH_3–ZrCl] and the subsequent transformation to [CH_2=ZrHCl], or that [CH_3–ZrCl] itself also absorbs UV light and converts to the methylidene complex. On the other hand, the early stages of annealing allow reaction of the Zr atom with methyl chloride, which shows that the insertion reaction proceeds without significant activation energy in the cold matrix, and that this reaction exothermicity also activates α-H transfer.

Zr + CH_3Br

The Zr + CH_3Br product spectra are shown in Figure 4, and are very similar to the Zr + CH_3Cl spectra in Figure 1. Clearly, the absorptions marked **I** increased and decreased upon irradiation with visible and near-UV light, respectively. The observed absorptions are assigned following the case of Zr + CH_3Cl. The absorptions marked **I** and **II** at 1556.6 and 1573.7 cm^{-1} (deuterium counterparts at 1117.1 and 1129.9 cm^{-1} in Figure 5, respectively, with H/D ratios of 1.393) are attributed to the Zr–H stretching mode. The absorption pair at 752.9 and 756.3 cm^{-1} are assigned to the C= Zr stretching mode. The deuterium counterparts are much weaker at 675.8 and 686.4 cm^{-1}, with H/D ratios of 1.114 and 1.102, respectively. The H/D ratios suggest that this mostly C=Zr stretching mode includes considerable displacement of the hydrogen atoms.

The much stronger absorptions marked **I** and **II** at 661.9 and 643.0 cm^{-1} in Figure 4 and 525.2 and 506.9 cm^{-1} in Figure 5, with H/D ratios of 1.260 and 1.271, respectively, are assigned to the CH_2 wagging mode. Weak absorptions marked **I** were observed at 622.6 and 614 cm^{-1}, and the **II** absorption was probably obscured by the precursor band centered at 602 cm^{-1}. These absorptions are attributed to the C–Zr–H bending mode. At the extreme low-frequency end, another absorption pair was observed at 482.7 and 453.6 cm^{-1}, whereas the deuterium counterparts were not observed because of their low frequencies. They are assigned to the CH_2 twisting mode. The observed vibrational characteristics indicate that [CH_2=ZrHBr] was formed in the reaction of Zr atoms with CH_3Br.

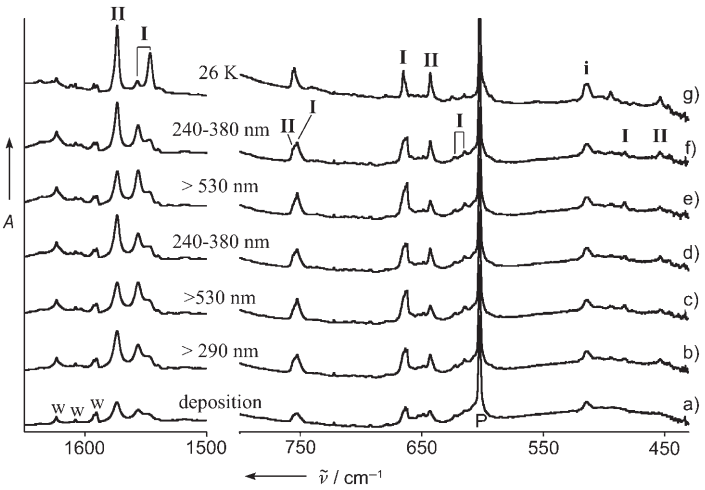

Figure 4. IR spectra in the regions of 1500–1650 and 430–800 cm^{-1} for laser-ablated Zr atoms codeposited with Ar/CH_3Br at 8 K. a) Zr + CH_3Br (0.2%) in Ar codeposited for 1 h. b) After broadband photolysis with a filter (>290 nm) for 30 min. c) After broadband photolysis with a filter (λ > 530 nm) for 30 min. d) After broad-band photolysis with a near-UV transmitting filter (240 < λ < 380 nm) for 30 min. e) After second photolysis with a filter (λ > 530 nm) for 30 min. f) After second photolysis with a near-UV transmitting filter (240 nm < λ < 380 nm) for 30 min. g) After annealing to 26 K. **I** and **II** refer to the absorption group arising from [CH_2=ZrHBr], and **i** refer to the absorption from CH_3-ZrBr.

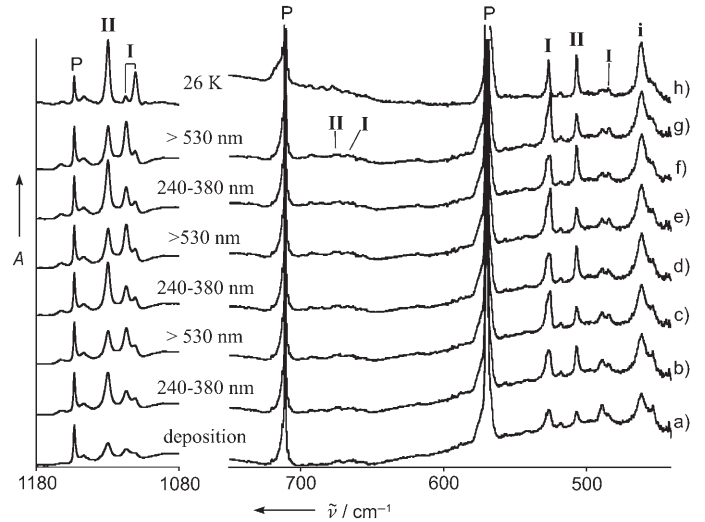

Figure 5. IR spectra in the regions of 1080–1180 and 440–750 cm^{-1} for laser-ablated Zr atoms codeposited with Ar/CD_3Br at 8 K. a) Zr + CD_3Br (0.5%) in Ar codeposited for 1 h. b) After broadband photolysis with a near-UV transmitting filter (240 < λ < 380 nm) for 30 min. c) After broadband photolysis with a filter (λ > 530 nm) for 30 min. d) After second photolysis with a near-UV transmitting filter (240 nm < λ < 380 nm) for 30 min. e) After second photolysis with a filter (λ > 530 nm) for 30 min. f) After third photolysis with a near-UV transmitting filter (240 nm < λ < 380 nm) for 30 min. g) After third photolysis with a filter (λ > 530 nm) for 30 min. h) After annealing to 26 K. **I** and **II** refer to the absorption group arising from [CH_2=ZrDCl], and **i** refers to the absorption from [CD_3–ZrCl].

 © 2006 Wiley-VCH Verlag GmbH & Co. KGaA, Weinheim

The observed spectroscopic characteristics of the **I** and **II** absorptions of [CH_2=ZrHBr] (Figures 4 and 5) are consistent with those for [CH_2=ZrHCl] (Figures 1 and 2). The observed difference in frequency of the Zr–H stretching absorption pair (17.1 cm^{-1}) in Figure 4 was slightly larger than that (16.5 cm^{-1}) in the Zr + CH_3Cl spectra, whereas the separations of other absorption pairs were slightly smaller. As in the case of [CH_2=ZrHCl], only one stable structure (C_1) was found in the singlet ground state for [CH_2=ZrHBr], but the planar structure is only 0.4 kcal mol^{-1} higher in energy. Calculations also showed that the lowest triplet state of [CH_2=ZrHBr] is 17.0 kcal mol^{-1} higher in energy than the singlet ground state and has a planar structure. Parallel to the case of singlet [CH_2=ZrHCl], the predicted vibrational characteristics for the planar (C_s) and C_1 structures of [CH_2=ZrHBr] are comparable to the **I** and **II** absorptions, respectively (Table 3).

The intensity of the absorption at 514.2 cm^{-1} marked **i** increased only slightly upon photolysis but more noticeably upon annealing. Upon annealing to 26 K, it became more than twice as strong as in the original spectrum after deposition. Two more absorptions showing the same behavior were observed at 1370.1 and 1129.0 cm^{-1} (not shown). The deuterium counterpart of the absorption at 514.2 cm^{-1} is located at 461.4 cm^{-1} (Figure 5). These absorptions are attributed to [CH_3–ZrBr] in the ground triplet state, in line with the case of Zr + CH_3Cl. The absorptions at 1370.1, 1129.0, and 524.2 cm^{-1} are assigned to the CH_3 bending, CH_3 deformation, and C–Zr stretching modes of [CH_3–ZrBr], respectively. The absorptions arising from triplet [CH_3-ZrBr] were also stronger relative to those of [CH_3–ZrF].[6] They gradually increased in intensity upon photolysis and later strengthened greatly upon annealing, a behavior similar to that for [CH_3–ZrCl].

In this study, the C–H bending and C–X stretching absorptions from the CH_2Cl (1389.8 and 826.1 cm^{-1}),[27] CHCl (814.5 cm^{-1}),[28] and CH_2Br (1354.9 and 692.1 cm^{-1})[29] radicals, fragments of the precursor by metal-plume radiation, were observed. They were relatively weak and remained unchanged upon photolysis but decreased in intensity upon annealing. The weak absorptions at 884.3 and 818.0 cm^{-1} arising from ZrO_2 and at 883.4 and 814.0 cm^{-1} from HfO_2 (not shown) were also observed,[30] and they increased in intensity upon photolysis and particularly upon annealing, which shows that unreacted metal atoms are present in the deposited samples.

Structures of the Zr complexes

The predicted structures of the Zr complexes at the level of B3LYP/6-311++G(3df,3pd) are shown in Figure 6, and the molecular parameters are listed in Table 5. [CH_3–ZrX] and [CH_2=ZrHX] have triplet and singlet ground electronic states, respectively. In the ground states, their structures retain C_s and C_1 symmetry (Figure 6) The methylzirconium halide complexes with F, Cl, and Br have C–Zr bond lengths of 2.229, 2.219, and 2.213 Å and C–Zr–X bond angles of 121.0, 124.9, and 126.1°, respectively. The measured C–Zr stretching frequency of the complexes increases in the same order (489.2, 513.9, and 514.2 cm^{-1}).

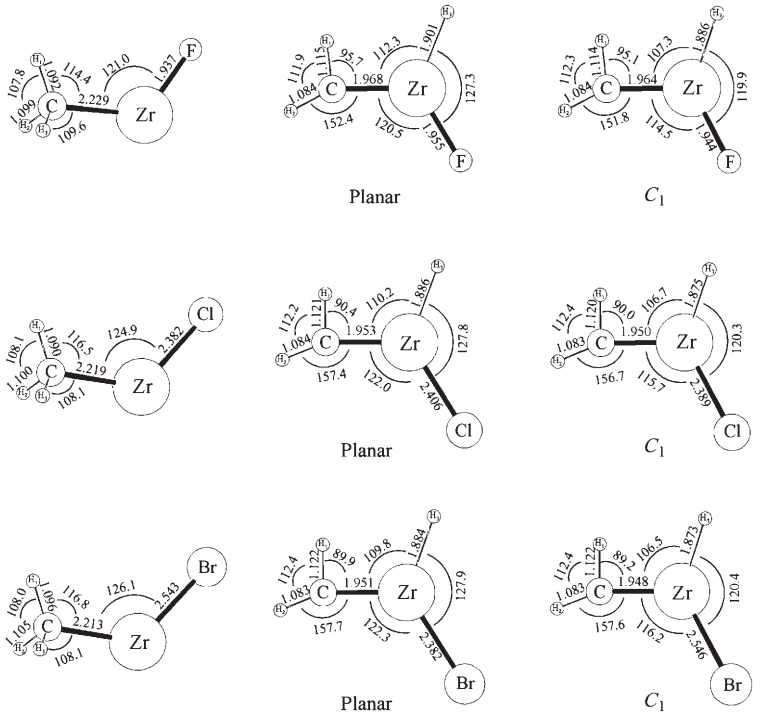

Figure 6. The optimized molecular structures of [CH_3–ZrX] (X = F, Cl, or Br) and [CH_2=ZrHX] (X = F, Cl, or Br) calculated with B3LYP||6-311++G(3df,3pd)|SDD. The bond lengths and angles are in Å and degrees, respectively.

The stable C_1 structures of the singlet methylidene complexes vary only slightly with the halogen atom, yet certain trends are notable. The methylidene structures with F, Cl, and Br show agostic C–H_1 bond lengths of 1.114, 1.120, and 1.122 Å, H_1···Zr distances of 2.342, 2.250, and 2.233 Å, C=Zr bond lengths of 1.964, 1.950, and 1.948 Å, Zr–H bond lengths of 1.886, 1.875, and 1.873 Å, and H_1–C–Zr bond angles of 95.1, 90.0, and 89.2°, respectively. The trends are

 © 2006 Wiley-VCH Verlag GmbH & Co. KGaA, Weinheim

CHEMISTRY
AN ASIAN JOURNAL

Table 5. Geometrical parameters and physical constants calculated for [CH_2=ZrHCl] (S), [CH_3–ZrCl] (T), [CH_2=ZrHBr] (S), and [CH_3<C-ZrBr] (T).[a]

Parameters	[CH_2=ZrHCl] (S)		[CH_3ZrCl] (T)	[CH_2=ZrHBr] (S)		[CH_3ZrBr] (T)
	Planar	C_1		Planar	C_1	
r(C–H_1)	1.121	1.120	1.090	1.122	1.122	1.096
r(C–H_2)	1.084	1.083	1.100	1.083	1.083	1.105
r(C–Zr)	1.953	1.950	2.219	1.951	1.948	2.213
r(Zr–H_3)	1.886	1.875		1.884	1.873	
r(Zr–X)	2.406	2.389	2.382	2.563	2.546	2.543
∡H_1CH_2	112.2	112.4	108.1	112.4	112.4	108.0
∡$CZrH_3$	110.2	106.7		109.8	106.5	
∡CZrX	122.0	115.7	124.9	122.3	116.2	126.1
∡H_3ZrX	127.8	120.3		127.9	120.4	
∡H_1CZr	90.4	90.0	116.5	89.9	89.2	116.8
∡H_2CZr	157.4	156.7	108.1	157.7	157.6	108.1
Φ(H_1CZrH_3)	0.0	18.1	121.9	0.0	16.5	122.0
Φ(H_1CZrX)	180.0	154.8	0.0	180.0	153.7	0.0
Φ(H_2CZrH_3)	180.0	−146.4	116.2	180.0	−148.0	116.0
Φ(H_2CZrX)	0.0	−9.6	121.9	0.0	−10.7	122.0
Mol symm	C_s	C_1	C_s	C_s	C_1	C_s
q(C)[b]	−0.77	−0.74	−0.89	−0.85	−0.77	−0.94
		(−1.00)			(−0.99)	
q(H_1)[b]	0.03	0.02	0.02	0.03	0.03	0.02
		(0.18)			(0.18)	
q(H_2)[b]	0.03	0.03	0.03	0.02	0.02	0.05
		(0.20)			(0.20)	
q(H_3)[b]	−0.45	−0.42	0.03	−0.43	−0.41	0.05
		(−0.44)			(−0.43)	
q(X)[b]	−0.83	−0.78	−0.82	−0.63	−0.63	−0.71
		(−0.50)			(−0.46)	
q(Zr)[b]	1.99	1.89	1.62	1.86	1.76	1.53
		(1.56)			(1.49)	
μ[c]	0.83	3.07	2.78	0.91	3.00	2.88
State[d]	$^1A'$	^1A	$^3A''$	$^1A'$	^1A	$^3A''$
ΔE[e]	93.2	94.0	96.8	91.3	92.0	95.7

[a] B3LYP/6-311++G(3df,3pd)/SDD level of theory. (S) and (T) denote singlet and triplet electronic states. Bond lengths and angles are in Å and degrees, respectively. [b] Mulliken atomic charge. The number in parentheses is the natural atomic charge. [c] Molecular dipole moment in D. [d] Electronic state. [e] Binding energies in kcal mol^{-1} relative to Zr($^3F_2$) and CH_3Cl or CH_3Br.

accompanied with the observed C=Zr stretching frequencies of 740.0, 749.1, and 752.9 cm^{-1} and the Zr–H stretching frequencies of 1537.8 (1551.3), 1554.0 (1570.5), and 1556.6 (1573.7) cm^{-1}, respectively, where the first numbers are the **I** frequencies and those in parentheses are the **II** values. The calculated and observed results are consistent, which indicates that both the C=Zr and Zr–H bonds become stronger in the order F, Cl, and Br, and the distortion of the CH_2 group increases. In other words, the methylidene complex becomes increasingly agostic in the order F, Cl, and Br, while the C=Zr and Zr–H bonds become stronger. The same result was observed in the CH_2=TiHX system.[8]

Two excellent review articles suggested that the agostic interaction arises from delocalization of the carbon–metal bonding electrons rather than the donation of electron density located on the alkyl substituent into a vacant orbital of the electron-deficient metal atom.[20,21] Therefore, the agostic interaction involves more than inclination of the C–H bond toward the metal atom, but rearrangement of the electron density and molecular structure around the carbon–metal bond. In this series, the halogen atoms are the source of the variation in the structural and vibrational characteristics, mostly by changing the electron density in the C=Zr bond. The computed Zr natural atomic charges[31] are 1.85, 1.56, and 1.49 with F, Cl, and Br, the halogen natural atomic charges are −0.67, −0.50, and −0.46, and the carbon charges are −1.07. −1.00, and −0.99, respectively, but the charges on H bonded to C are not changed (±0.001). This shows that electron density flows from halogen and carbon to the electron-deficient metal center as the agostic interaction, and the C=Zr bond strength increases. A higher electron density in the C=Zr bond leads to a shorter bond and higher stretching frequency, which in turn allows more delocalization of the electron density, thus resulting in a stronger Zr–H bond and more distortion of the CH_2 group. Clearly, the agostic interaction involves more than coordination of a C–H bond to an electron-deficient metal center. In this series, the most electron-deficient metal center (highest natural positive charge) supports the weakest agostic interaction. The apparent inductive effect of the halogen substituents on the structure and vibrational characteristics of the methylidene complexes accounts for the trend in agostic bonding and provides an interesting subject for future theoretical investigation.

Hf + CH_3Cl

The spectra of Hf + CH_3Cl and HF + CD_3Cl in an Ar matrix after deposition, photolysis, and annealing are shown in Figures 7 and 8, respectively. These spectra are similar to the spectra of Zr in Figures 1and 2, but the frequencies of the product absorptions are higher (Table 6). The higher frequencies of Hf complexes relative to those of Zr complexes were also observed in previous studies,[4–7] and originate from the large relativistic contraction in bond length for Hf as predicted by Pyykkö et al.[32] Two groups of absorptions marked **I** and **II** arising from the methylidene complex were also observed side by side, while only one group of absorptions was observed in a Ne matrix, consistent with the Zr cases.

The absorptions at 1615.0 cm^{-1} marked **I** increased by about 20% upon irradiation with visible light, whereas the one at 1641.6 cm^{-1} marked **II** decreased by about 10%. After near-UV photolysis, **I** slightly decreased, whereas **II**

 © 2006 Wiley-VCH Verlag GmbH & Co. KGaA, Weinheim

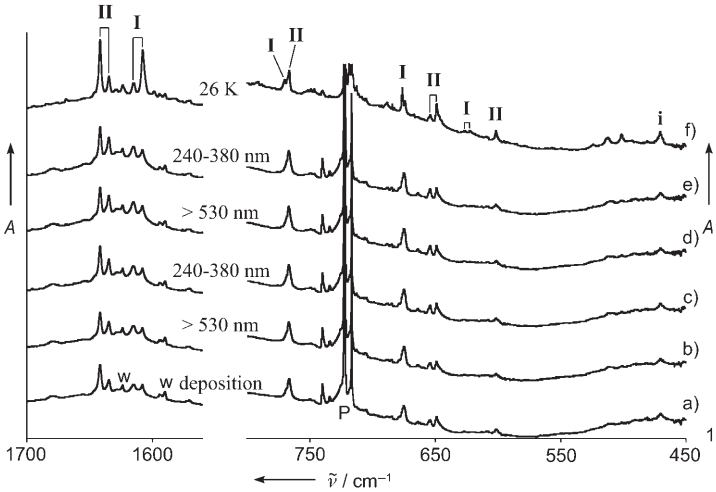

Figure 7. IR spectra in the regions of 1560–1700 and 450–800 cm^{-1} for laser-ablated Hf atoms codeposited with Ar/CH_3Cl at 8 K. a) Hf + CH_3Cl (0.2%) in Ar codeposited for 1 h. b) After broadband photolysis with a filter ($\lambda > 530$ nm) for 20 min. c) After broadband photolysis with a near-UV transmitting filter ($240 < \lambda < 380$ nm) for 20 min. d) After second photolysis with a filter ($\lambda > 530$ nm) for 20 min. e) After second photolysis with a near-UV transmitting filter (240 nm $< \lambda < 380$ nm) for 20 min. f) After annealing to 26 K. **I** and **II** refer to the absorption group arising from [CH_2=HfHCl], and **i** refer to the absorption from [CH_3–HfCl].

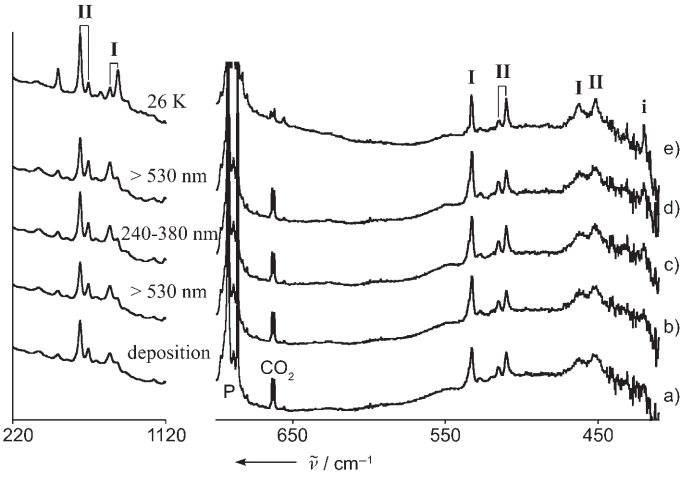

Figure 8. IR spectra in the regions of 1120–1220 and 410–700 cm^{-1} for laser-ablated Hf atoms codeposited with Ar/CD_3Cl at 8 K. a) Hf + CD_3Cl (0.5%) in Ar codeposited for 1 h. b) After broadband photolysis with a filter ($\lambda > 530$ nm) for 20 min. c) After broadband photolysis with a near-UV transmitting filter ($240 < \lambda < 380$ nm) for 20 min. d) After second photolysis with a filter ($\lambda > 530$ nm) for 20 min. e) After annealing to 26 K. **I** and **II** refer to the absorption group arising from [CH_2=HfDCl], and **i** refers to the absorption from [CD_3–HfCl].

Table 6. Frequencies of observed product absorptions from reactions of Hf with methyl halides.[a]

Hf + CH_3Cl			Hf + CD_3Cl			Hf + CH_3Br		Hf + CD_3Br		Description
Ne	Ar		Ne	Ar		Ar		Ar		
	I	**II**		**I**	**II**	**I**	**II**	**I**	**II**	
1630.7	1615.0,	**1641.6**,	1182.5	1156.5,	**1175.9**,	1619.1,	**1644.3**,	1159.2,	**1177.8**,	Hf–H stretch
	1607.8	1634.7		**1151.3**	1170.5	**1609.7**	1635.7	**1152.5**	1171.2	
770.7	766.9	766.3		[b]	[b]	769.1	767.6	696.2	697.7	C=Hf stretch
677.7	676.1,	653.9,	520.8	**532.8**,	515.0,	674.4	653.7,	533.4,	515.3,	CH_2 wag
	674.5	**648.8**		532.1	**510.0**		**649.0**	**532.0**	**510.3**	
	626.1,	601.4	464.5	462.6	451.6	**622.5**,	[b]	461.6	452.9	C–Hf–H bend
	622.0					619.5				
	1385.0, 1380.2			1010.3		**1381.4**, 1376.5		**1008.3**, 1004.9		CH_3 scissors
1161.1	1155.9, **1152.8**			899.2		1154, 1153.4,		895.9		CH_3 deform
						1150.5				
478.7	470.1		418.4	419.4		473.1		419.2		C–Hf stretch

[a] All frequencies are in cm^{-1}. Stronger absorptions are in bold. The methylidene product is listed in the top portion followed by the insertion product. [b] Obscured by precursor absorption.

increased by about 30%. The variations in intensity were repeated when the Hf complexes were re-irradiated with visible and near-UV light. This photoreversibility of absorptions is similar to the Zr cases, but the variations in intensity for Hf are far smaller. Upon annealing, the absorption at 1615.0 cm^{-1} decreased while the absorption at 1607.8 cm^{-1}, also marked **I**, increased dramatically.

The observed absorptions are assigned according to the Zr cases. The paired absorptions at 1607.8 and 1641.6 cm^{-1} have their deuterium counterparts at 1151.3 and 1175.9 cm^{-1} (H/D ratios of 1.397 and 1.396), respectively, and are attributed to the Hf–H stretching mode of the major product. In previous studies, the Hf–H stretching absorptions of hafnium hydrides, which were not observed in this study, were observed in the same frequency region.[24] The heavily overlapping absorptions at 766.9 and 766.3 cm^{-1} (the deuterium counterparts overlap with a precursor absorption) are assigned to the mostly C=Hf stretching mode. The absorptions at 674.5 and 648.8 cm^{-1} have deuterium counterparts at 532.8 and 510.0 cm^{-1} (H/D ratios of 1.266 and 1.272), respectively, and are attributed to the CH_2 wagging mode. The absorptions at 626.1 and 601.4 cm^{-1} have their deuterium counterparts at 462.6 and 451.6 cm^{-1} (H/D ratios of 1.353 and 1.332), respectively, and are attributed to the C–Hf–H bending mode.

The present results indicate that both **I** and **II** absorptions arise from the methylidene complex [CH_2=HfHCl], which is a major product in the reaction of Hf with CH_3Cl, and is consistent with a previous study of Hf + CH_3F.[4] Calculations, however, showed that there is only one stable structure (C_1) at the present level of theory. As with the Zr cases, the frequency of the Hf–H **I** stretching absorption is lower than that of the **II**, but the frequencies of the C=Hf stretching absorptions are comparable. The other **I** frequencies are higher than the **II** frequencies (Table 6).

The predicted vibrational characteristics for the stable C_1 structure match the observed values of the **II** absorptions, whereas those of the planar structure, which is only 0.8 kcal

 © 2006 Wiley-VCH Verlag GmbH & Co. KGaA, Weinheim

mol^{-1} higher, are comparable to observed values of the **I** absorptions (Table 7). Reversion to the nonplanar structure via the imaginary out-of-plane Hf–H bending mode is prevented by the matrix cage. No other structures of the methylidene complex reproduce the observed vibrational characteristics of the **I** absorptions relative to those of **II**. The lowest triplet state, which is 13 kcal mol^{-1} higher and accessed upon photolysis, enables the planar structure to be preserved in the matrix even after relaxation to the ground electronic state.

Another absorption marked **i** is observed at 470.1 cm^{-1}, whose intensity remains almost unchanged in the cycles of visible and near-UV photolysis, but doubles in the early stages of annealing. Two more absorptions with the same behavior were observed at 1385.0 and 1152.8 cm^{-1} (not shown). Consistent with the Zr cases, the three bands at 1385.0, 1152.8, and 470.1 cm^{-1} are assigned to the CH_3 bending, CH_3 deformation, and C–Hf stretching modes of triplet [CH_3–HfCl]. They are in fact the strongest observable modes predicted for the insertion complex (Table 8). [CH_3–HfF] was not identified in the previous reaction of Hf with CH_3F.[4] This indicates that, in agreement with the Zr cases, the chloride complex ([CH_3–HfCl]) is more stable than the fluoride, each relative to the corresponding methylidene complexes.

Hf + CH_3Br

The spectra for Hf + CH_3Br shown in Figures 9 and 10 are very similar to those for CH_3Cl, thus suggesting that CH_2=HfHBr is again the major product. The intensities of the absorptions marked **II** increased upon near-UV irradiation but stay almost unchanged upon irradiation with visible light. On the other hand, those of **I** increased only slightly upon photolysis but dramatically on annealing. The absorptions are assigned following the case of Hf + CH_3Cl: the pair at 1609.7 and 1644.3 cm^{-1} to the Hf–H stretching mode, the ones at 769.1 and 767.6 cm^{-1} to the C=Hf stretching mode, the bands at 674.4 and 649.0 cm^{-1} to the CH_2 wagging mode, and the peak at 622.5 cm^{-1} to the C–Hf–H bending mode. The observed frequencies of [CH_2=HfHBr] are compared with the predicted values for the planar (C_s) and C_1 stable structures in the singlet ground state in Table 7. The planar structure in the ground singlet state is 0.7 kcal mol^{-1} higher

Table 7. Observed and calculated fundamental frequencies of [CH_2=HfHCl] and [CH_2=HfHBr] in the ground electronic states (^{1}A).[a]

Description	[CH_2=HfHCl]					[CD_2=HfDCl]					[CH_2=HfHBr]					[CD_2=HfDBr]				
	Exp		Calcd		I	Exp		Calcd		I	Exp		Calcd		I	Exp		Calcd		I
	I	II	Planar	C_1		I	II	Planar	C_1		I	II	Planar	C_1		I	II	Planar	C_1	
C–H_b stretch			3196.0	3195.6	0			2363.3	2363.2	2			3195.8	3196.2	0			2363.3	2363.7	2
C–H_a stretch			2804.3	2833.5	9			2043.1	2063.6	3			2802.0	2819.3	8			2041.2	2053.3	3
Hf–H_c stretch	1607.8	1641.6	1650.8	1671.4	291	1151.3	1175.9	1171.3	1186.0	149	1644.3	1644.3	1654.8	1672.3	300	1153.5	1177.8	1174.1	1186.5	154
CH_2 scissors			1345.7	1334.3	18			1031.0	1024.3	18			1342.8	1338.0	19			1029.4	1026.1	19
C=Hf stretch	766.9	766.3	768.2	760.6	58	[b]	[b]	688.5	681.7	42	769.1	767.6	767.8	763.6	61	696.2	697.7	687.9	684.8	45
CH_2 wag	674.5	648.8	723.0	694.9	115	532.8	510.0	569.0	543.3	83	674.4	649.0	722.6	697.4	115	532.0	510.3	564.8	545.1	83
C–Hf–H_c bend	626.1	601.4	609.5	600.0	56	462.6	451.6	459.6	447.1	47	622.5	[b]	606.8	605.0	44	461.6	452.9	453.9	447.5	29
CH_2 twist			496.6	431.5	54			352.2	350.0	48			482.0	433.5	45			341.7	308.3	23
CH_2 rock			405.4	369.0	3			339.0	302.5	16			397.2	386.0	6			298.6	292.6	4
Hf–X stretch			342.8	350.8	52			304.4	282.6	3			232.2	242.2	50			229.8	236.8	27
Hf–H_c OOP bend			−125.8	224.6	65			−93.4	166.8	29		–	−128.7	207.4	49			−94.2	155.0	27
C–Hf–X bend			127.7	111.2	20			114.6	98.2	17			113.5	100.6	17			101.0	88.5	15

[a] Observed frequencies were all measured in an Ar matrix. B3LYP/6-311++G(2d,p)/SDD(Zr) calculations were used. Frequencies and intensities are in cm^{-1} and km mol^{-1}, and ^{35}Cl and ^{79}Br were assumed in calculations. [b] Obscured by precursor absorption.

Table 8. Observed and calculated fundamental frequencies of [CH_3HfCl] and [CH_3HfBr] isotopomers in the ground electronic states (^{3}A).[a]

Description	[CH_3HfCl]			I	[CD_3HfCl]		I	[CH_3HfBr]			I	[CD_3HfBr]		I
	Exp	MP2	Calcd		Exp	Calcd		Exp	MP2	Calcd		Exp	Calcd	
A′ CH_3 stretch		3156.4	3078.7	3		2272.3	2		3155.5	3081.3	3		2274.4	1
A′ CH_3 stretch		3011.0	2956.3	6		2123.0	1		3010.5	2958.9	6		2124.6	1
A′ CH_3 scissors		1413.9	1414.2	3		1025.7	2		1410.5	1412.7	3		1024.7	2
A′ CH_3 deform	1152.8	1157.6	1167.4	18	899.2	915.6	28	1150.5	1156.0	1164.9	19	895.9	913.9	30
A′ C–Hf stretch	470.1	517.6	503.1	25	419.4	439.5	23	473.1	515.8	500.3	31	419.2	438.0	29
A′ Hf–X stretch		377.5	397.2	33		347.3	59		355.9	387.1	21		302.7	13
A′ CH_3 rock		340.5	337.6	39		300.5	1		235.2	228.2	23		226.2	20
A′ C–Hf–X bend		74.4	81.2	0		74.8	0		64.3	69.7	0		62.9	0
A″ CH_3 stretch		3096.4	3013.5	4		2225.2	1		3096.3	3017.1	3		2227.8	1
A″ CH_2 bend	1385.0	1413.4	1418.1	8	1010.3	1028.6	5	1381.4	1411.2	1417.0	8	1008.3	1027.9	5
A″ CH_3 rock		366.5	385.9	2		287.8	2		357.4	381.0	2		284.6	2
A″ CH_3 distort		91.9	96.5	1		70.0	0		83.1	84.1	1		61.5	0

[a] Observed frequencies were all measured in an Ar matrix. B3LYP/6-311++G(2d,p)/SDD(Zr) calculations are given with MP2 added for comparison. Frequencies and intensities are in cm^{-1} and km mol^{-1}, and ^{35}Cl and ^{79}Br were assumed in calculations.

© 2006 Wiley-VCH Verlag GmbH & Co. KGaA, Weinheim

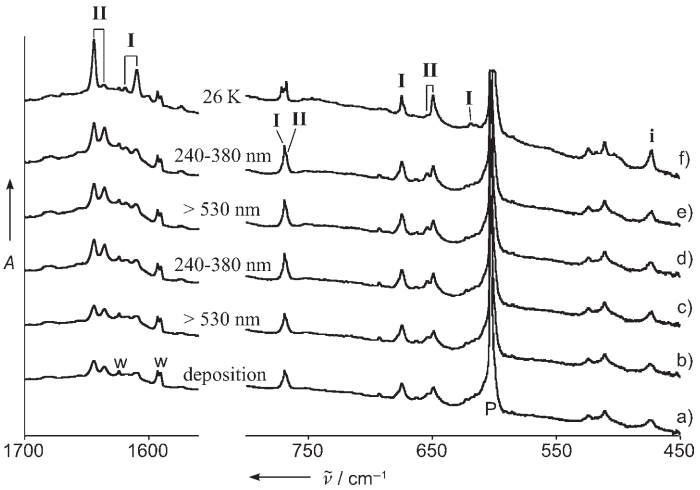

Figure 9. IR spectra in the regions of 1560–1700 and 450–800 cm^{-1} for laser-ablated Hf atoms codeposited with Ar/CH_3Br at 8 K. a) Hf + CH_3Br (0.2%) in Ar codeposited for 1 h. b) After broadband photolysis with a filter ($\lambda > 530$ nm) for 20 min. c) After broadband photolysis with a near-UV transmitting filter ($240 < \lambda < 380$ nm) for 20 min. d) After second photolysis with a filter ($\lambda > 530$ nm) for 20 min. e) After second photolysis with a near-UV transmitting filter (240 nm $< \lambda <$ 380 nm) for 20 min. f) After annealing to 26 K. **I** and **II** refer to the absorption group arising from [CH_2=HfHBr], and **i** refers to the absorption from [CH_3–HfBr].

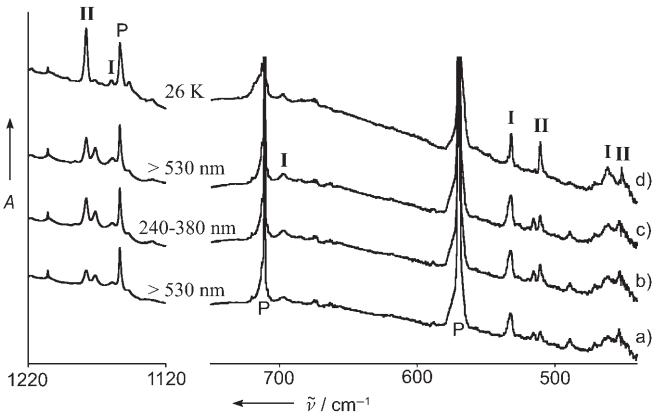

Figure 10. IR spectra in the regions of 1120–1220 and 440–700 cm^{-1} for laser-ablated Hf atoms codeposited with Ar/CD_3Br at 8 K. a) Hf + CD_3Br (0.5%) in Ar codeposited for 1 h followed by broadband photolysis with a filter ($\lambda > 530$ nm) for 20 min. b) After broadband photolysis with a near-UV transmitting filter ($240 < \lambda < 380$ nm) for 20 min. c) After second photolysis with a filter ($\lambda > 530$ nm) for 20 min. d) After annealing to 26 K. **I** and **II** refer to the absorption group arising from [CH_2=HfDBr], and **i** refers to the absorption from [CD_3–HfBr].

in energy than the C_1 structure, and the lowest triplet state, which has a planar structure, is 13 kcal mol^{-1} higher in energy.

The absorption at 473.1 cm^{-1} and two associated absorptions at 1381.4 and 1150.5 cm^{-1} (not shown) increased upon photolysis, and increased by almost 100% upon annealing. These absorptions are attributed to [CH_3–HfBr]. Figure 9 also shows that the [CH_3–HfBr] absorptions are stronger than those for [CH_3–HfCl]. The Grignard-type complex was not identified from the Hf + CH_3F reaction, which suggests that the [CH_3–HfF] first formed in the reaction of Hf with CH_3F was rearranged to the high-oxidation-state complex [CH_2=HfHF]. Calculations showed that, as with the Zr case, the methylhafnium halide complexes are essentially equal in energy relative to the methylidene complex; the energies of the methylhafnium halide and methylidene complexes are within 1 kcal mol^{-1} with F, Cl, and Br substituents.

Structures of the Hf complexes

The predicted structures for the Hf complexes at the level of B3LYP/6-311++G(3df,3pd) are shown in Figure 11, and the molecular parameters are listed in Table 9. The methyl

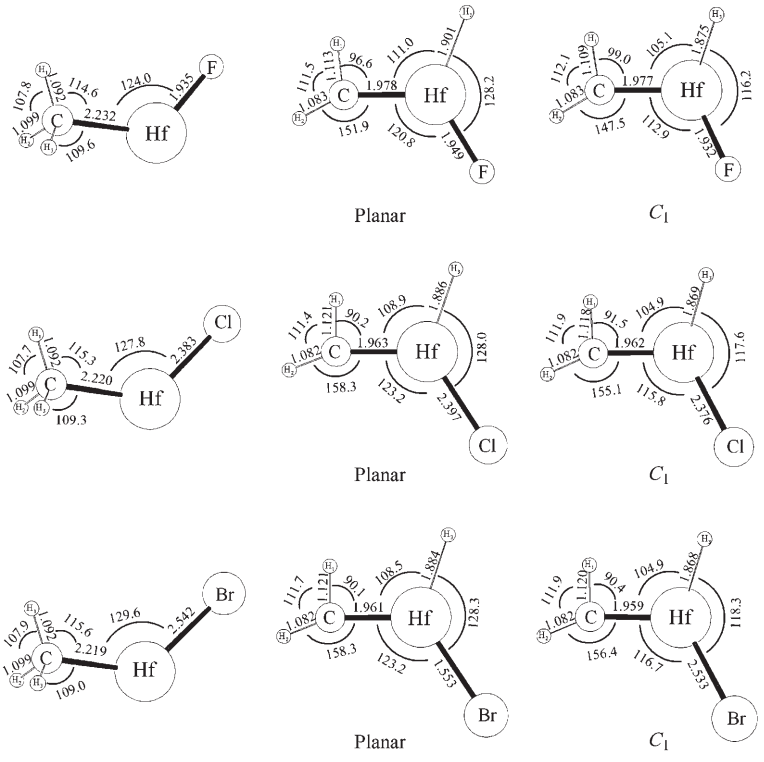

Figure 11. The optimized molecular structures of [CH_3–HfX] (X = F, Cl, or Br) and [CH_2=HfHX] (X = F, Cl, or Br) complexes calculated with B3LYP||6-311++G(3df,3pd)|SDD. The bond lengths and angles are in Å and degrees, respectively.

 © 2006 Wiley-VCH Verlag GmbH & Co. KGaA, Weinheim

CHEMISTRY
AN ASIAN JOURNAL

Table 9. Geometrical parameters and physical constants calculated for [CH_2=HfHCl] (S), [CH_3HfCl] (T), [CH_2=HfHBr] (S), and [CH_3HfBr] (T).[a]

Parameters	[CH_2=HfHCl] (S)		[CH_3HfCl] (T)	[CH_2=HfHBr]1 (S)		[CH_3HfBr] (T)
	Planar	C_1		Planar	C_1	
r(C−H_1)	1.121	1.118	1.092	1.121	1.120	1.092
r(C−H_2)	1.082	1.082	1.099	1.082	1.082	1.099
r(C−Hf)	1.963	1.962	2.220	1.961	1.959	2.219
r(Hf−H_3)	1.886	1.869		1.884	1.868	
r(Hf−X)	2.397	2.376	2.383	1.553	2.533	2.542
∡H_1CH_2	111.4	111.9	107.7	111.7	111.9	107.9
∡$CHfH_3$	108.9	104.9		108.5	104.9	
∡CHfX	123.2	115.8	127.8	123.2	116.7	129.6
∡H_3HfX	128.0	117.6		128.3	118.3	
∡H_1CHf	90.2	91.5	115.3	90.1	90.4	115.6
∡H_2CHf	158.3	155.1	109.3	158.3	156.4	109.0
Φ(H_1CHfH_3)	0.0	20.1	121.5	0.0	17.8	121.6
Φ(H_1CHfX)	180.0	151.4	0.0	180.0	150.9	0.0
Φ(H_2CHfH_3)	180.0	−140.9	117.0	180.0	−143.7	116.8
Φ(H_2CHfX)	0.0	−9.6	121.5	0.0	−10.6	121.5
Mol symm	C_s	C_1	C_s	C_s	C_1	C_s
q(C)[b]	−0.66	−0.62	−0.89	−0.64	−0.60	−0.77
		(−1.11)			(−1.09)	
q(H_1)[b]	0.03	0.00	0.06	0.02	0.01	0.02
		(0.19)			(0.19)	
q(H_2)[b]	0.07	0.06	0.09	0.08	0.06	0.05
		(0.20)			(0.20)	
q(H_3)[b]	−0.38	−0.33	0.09	−0.36	−0.32	0.05
		(−0.46)			(−0.45)	
q(X)[b]	−0.80	−0.76	−0.78	−0.57	−0.58	−0.62
		(−0.51)			(−0.47)	
q(Hf)[b]	1.74	1.65	1.43	1.47	1.42	1.27
		(1.68)			(1.62)	
μ[c]	0.76	3.32	2.38	0.76	3.14	2.47
State[d]	$^1A'$	^1A	$^3A''$	$^1A'$	^1A	$^3A''$
ΔE[e]	89.7	90.1	91.1	88.1	88.5	89.5

[a] B3LYP/6-311++G(3df,3pd)/SDD level of theory. (S) and (T) denote singlet and triplet electronic states. Bond lengths and angles are in Å and degrees, respectively. [b] Mulliken atomic charge. The number in parentheses is the natural atomic charge. [c] Molecular dipole moment in D. [d] Electronic state. [e] Binding energies in kcal mol^{-1} relative to Hf($^3F_2$) and CH_3Cl or CH_3Br.

metal halide and methylidene complexes have the triplet and singlet ground electronic states with C_s and C_1 symmetry, respectively, consistent with the Zr cases.

The variations in structure of the Hf methylidene with the halogen atoms are similar to those observed for the Zr methylidene complexes. The structures with F, Cl, and Br show agostic C−H_1 bond lengths of 1.109, 1.118, and 1.120 Å, H_1···Hf distances of 2.413, 2.284, and 2.260 Å, C=Hf bond lengths of 1.977, 1.962, and 1.959 Å, Hf−H bond lengths of 1.874,1.869, and 1.868 Å, and H_1−C−Hf bond angles of 99.0, 91.5, and 90.4°, respectively. In this series, the Hf natural atomic charges are 1.96, 1.68, and 1.62 with F, Cl, and Br, the halogen natural atomic charges are −0.69, −0.51, and −0.47, and the carbon charges are −1.17, −1.11, and −1.09, respectively, but the H_1 and H_2 charges are not changed. A higher electron density in the C=Hf bond leads to a shorter bond length and higher stretching frequency, which is most probably accompanied by a higher extent of delocalization of the electron density to the rest of the molecule. This in turn results in a stronger Hf−H bond and more distortion of the CH_2 group, as discussed for the Zr complexes. In summary, the Group IV (Ti, Zr, and Hf) methylidene complexes [CH_2=MHX] all become more agostic in the order F, Cl, and Br.

Conclusions

Reactions of laser-ablated Zr and Hf atoms with methyl chloride and bromide in an excess of Ne, Ar, or Kr have been carried out during condensation. Two major products, the methylidene [CH_2=MHX] (X = Cl or Br) and methyl metal halide [CH_3−MX] complexes, were identified in the IR spectra. Whereas the amount of both products increased upon photolysis, that of the methyl metal halide increased substantially upon annealing, in contrast to the low yield of the methyl fluoride complexes [CH_3−MF] studied previously,[4,6] which shows that this insertion reaction is spontaneous and requires little or no activation energy.

Two sets of absorptions from the methylidene complex in Ar and Kr matrices were observed side by side with up to 37 cm^{-1} separation, but only one set was observed in the spectra for the Ne matrix. The two sets of absorptions form a persistent photoreversible system in the Zr spectra. Upon irradiation with visible light, the intensiites of **I** absorptions increased but those of **II** decreased; near-UV irradiation reversed the effect. In the case of the Hf complex, the variations in intensity of the two sets of absorptions were much smaller. Calculations for a planar methylidene complex in the singlet ground state reproduced the characteristics of the **I** absorptions, whereas the vibrational characteristics of the more stable C_1 structure matched those of the **II** absorptions, which means that the matrix traps methylidene complexes in nearly planar and pyramidal forms.

The agostic interaction in the methylidene complexes increases with the substituents F, Cl, and Br, in that order. Computed natural electron charges revealed a flow from carbon and halogen atoms to the metal centers that is consistent with the halogen inductive effect. The C=M and M−H stretching frequencies increased and the bond lengths decreased with the distortion of the CH_2 group. The same trend was also observed in the [CH_2=TiHX] system.[2,8] A higher electron density in the C=M bond not only strengthens the bond, but is accompanied by a more agostic distor-

 © 2006 Wiley-VCH Verlag GmbH & Co. KGaA, Weinheim

tion and a stronger M–H bond as well. The consistent variation of the molecular structure around the C=M bond and the vibrational frequencies with halogen substituents follow charge reorganization and support recent descriptions of the agostic interaction.[20,21] This interaction involves more than electron donation from the nearby C–H bond to the metal center; it includes charge reorganization and molecular structural rearrangement to stabilize the carbon–metal bond.

Experimental and Calculational Methods

CH_3Cl, CH_3Br, CD_3Br (Cambridge Isotope Laboratories, 99%), and CD_3Cl (synthesized from $HgCl_2$ and CD_3Br) were used to react with laser-ablated Zr and Hf atoms (Johnson-Matthey) in excess Ne, Ar, or Kr during condensation at 8 K with a closed-cycle He refrigerator (Air Products). The methods were described in detail elsewhere.[2–7,22] Concentrations of gas mixtures were typically 0.2–0.5%. After reaction, IR spectra were recorded at a resolution of 0.5 cm^{-1} with a Nicolet 550 spectrometer with an HgCdTe detector. Samples were later irradiated by a combination of an optical filter ($\lambda > 530$ nm or $240 < \lambda < 380$ nm) and a mercury arc lamp (175 W, globe removed) and were annealed, after which more spectra were recorded.

Complementary density functional theory (DFT) calculations were carried out with the Gaussian 03 package.[23] B3LYP density functional 6-311++G(2dp) basis sets for C, H, Cl, and Br and SDD pseudopotential and basis sets for Zr and Hf were obtained to provide a consistent set of vibrational frequencies for the reaction products. For confirmation of the B3LYP results, MP2, BPW91, and CCSD calculations were also carried out with the same basis sets. Geometries were fully relaxed during optimization, and the optimized geometries were confirmed by vibrational analysis. The illustrated structures were calculated with the large 6-311++G(3df,3pd) basis set. All vibrational frequencies were calculated analytically. In the calculation of the binding energy of a metal complex, the zero-point energy was included.

Acknowledgements

We gratefully acknowledge financial support from NSF Grant CHE 03-52487 to L.A. and the assistance of X. Wang with neon-matrix experiments.

[1] R. R. Schrock, *Chem. Rev.* **2002**, *102*, 145.
[2] Ti+CH_3F: H.-G. Cho, L. Andrews, *J. Phys. Chem. A* **2004**, *108*, 6294.
[3] Ti+CH_4: L. Andrews, H.-G Cho, X. Wang, *Inorg. Chem.* **2005**, *44*, 4834.
[4] Hf+CH_3F: H.-G. Cho, L. Andrews, *Organometallics* **2004**, *23*, 4357.
[5] Hf+CH_4: H.-G Cho, X. Wang, L. Andrews, *Organometallics* **2005**, *24*, 2854.
[6] Zr+CH_3F: H.-G. Cho, L. Andrews, *J. Am. Chem. Soc.* **2004**, *126*, 10485.
[7] Zr+CH_4: H.-G Cho, X. Wang, L. Andrews, *J. Am. Chem. Soc.* **2005**, *127*, 465.
[8] Ti+CH_3X: H.-G. Cho, L. Andrews, *Inorg. Chem.* **2005**, *44*, 979.
[9] Mo+CH_4: H.-G. Cho, L. Andrews, *J. Am. Chem. Soc.* **2005**, *127*, 8226.
[10] Mo+CH_3F: H.-G. Cho, L. Andrews, *Chem. Eur. J.* **2005**, *11*, 5017.
[11] W+CH_4: H.-G. Cho, L. Andrews, C. Marsden, *Inorg. Chem.* **2005**, *44*, 7634.
[12] Cr and W+CH_3F: H.-G. Cho, L. Andrews, *Organometallics* **2005**, *24*, 5678.
[13] Nb+CH_3F: H.-G. Cho, L. Andrews, *Organometallics* **2006**, *25*, 477.
[14] V, Nb, and Ta+CH_4: H.-G. Cho, L. Andrews, *J. Phys. Chem. A* **2006**, *110*, 3886.
[15] M. R. Buchmeiser, *Chem. Rev.* **2000**, *100*, 1565.
[16] R. H. Crabtree, *Chem. Rev.* **1995**, *95*, 987, and references therein.
[17] K. Wada, B. Craig, C. B. Pamplin, P. Legzdins, B. O. Patrick, I. Tsyba, R. Bau, *J. Am. Chem. Soc.* **2003**, *125*, 7035.
[18] M. Brookhart, M. L. H. Green, *J. Organomet. Chem.* **1983**, *250*, 395.
[19] G. Ujaque, A. C. Cooper, F. Maseras, O. Eisenstein, K. G. Caulton, *J. Am. Chem. Soc.* **1998**, *120*, 361.
[20] E. Clot, O. Eisenstein in *Computational Inorganic Chemistry* (Eds.: N. Kaltzoyannis, J. E. McGrady), *Structure and Bonding*, Springer, Heidelberg, **2004**, pp. 1–36.
[21] W. Scherer, G. S. McGrady, *Angew. Chem.* **2004**, *116*, 1816; *Angew. Chem. Int. Ed.* **2004**, *43*, 1782.
[22] L. Andrews, *Chem. Soc. Rev.* **2004**, *33*, 123, and references therein.
[23] K. N. Kudin, J. C. Burant, J. M. Millam, S. S. Iyengar, J. Tomasi, V. Barone, B. Mennucci, M. Cossi, G. Scalmani, N. Rega, G. A. Petersson, H. Nakatsuji, M. Hada, M. Ehara, K. Toyota, R. Fukuda, J. Hasegawa, M. Ishida, T. Nakajima, Y. Honda, O. Kitao, H. Nakai, M. Klene, X. Li, J. E. Knox, H. P. Hratchian, J. B. Cross, C. Adamo, J. Jaramillo, R. Gomperts, R. E. Stratmann, O. Yazyev, A. J. Austin, R. Cammi, C. Pomelli, J. W. Ochterski, P. Y. Ayala, K. Morokuma, G. A. Voth, P. Salvador, J. J. Dannenberg, V. G. Zakrzewski, S. Dapprich, A. D. Daniels, M. C. Strain, O. Farkas, D. K. Malick, A. D. Rabuck, K. Raghavachari, J. B. Foresman, J. V. Ortiz, Q. Cui, A. G. Baboul, S. Clifford, J. Cioslowski, B. B. Stefanov, G. Liu, A. Liashenko, P. Piskorz, I. Komaromi, R. L. Martin, D. J. Fox, T. Keith, M. A. Al-Laham, C. Y. Peng, A. Nanayakkara, M. Challacombe, P. M. W. Gill, B. Johnson, W. Chen, M. W. Wong, C. Gonzalez, J. A. Pople, Gaussian 03, Revision B.04, Gaussian, Inc., Pittsburgh, **2003**, and references therein.
[24] ZrH_4 and HfH_4: G. V. Chertihin, L. Andrews, *J. Phys. Chem.* **1995**, *99*, 15004.
[25] R. J. H. Clark, B. K. Hunter, D. M. Rippon, *Inorg. Chem.* **1972**, *11*, 56.
[26] M. E. Jacox, *Chem. Phys.* **1994**, *189*, 149.
[27] CH_2Cl: a) L. Andrews, D. W. Smith, *J. Chem. Phys.* **1970**, *53*, 2956; b) M. E. Jacox, D. E. Milligan, *J. Chem. Phys.* **1970**, *53*, 2688; c) T. D. Fridgen, X. K. Zhang, J. M. Parnis, R. E. March, *J. Phys. Chem. A* **2000**, *104*, 3487.
[28] CHCl: M. E. Jacox, D. E. Milligan, *J. Chem. Phys.* **1967**, *47*, 1626.
[29] CH_2Br: D. W. Smith, L. Andrews, *J. Chem. Phys.* **1971**, *55*, 5295.
[30] ZrO_2 and HfO_2: G. V. Chertihin, L. Andrews, *J. Phys. Chem.* **1995**, *99*, 6356.
[31] A. E. Reed, L. A. Curtiss, F. Weinhold, *Chem. Rev.* **1988**, *88*, 899.
[32] a) P. Pyykkö, J. P. Desclaux, *Chem. Phys. Lett.* **1977**, *50*, 503; b) P. Pyykkö, J. G. Snijders, E. Baerends, *Chem. Phys. Lett.* **1981**, *83*, 432; c) T. Ziegler, J. G. Snijders, E. J. Baerends, *J. Chem. Phys.* **1981**, *74*, 1271; d) P. Pyykkö, *Chem. Rev.* **1988**, *88*, 563.

Received: February 3, 2006
Published online: July 12, 2006

 © 2006 Wiley-VCH Verlag GmbH & Co. KGaA, Weinheim